How to cite: *Angew. Chem. Int. Ed.* **2023**, *62*, e202311181
doi.org/10.1002/anie.202311181

Photopharmacology **Hot Paper**

Three-Photon Infrared Stimulation of Endogenous Neuroreceptors in Vivo

Rosalba Sortino, Marina Cunquero, Gustavo Castro-Olvera, Ricard Gelabert, Miquel Moreno, Fabio Riefolo, Carlo Matera, Noèlia Fernàndez-Castillo, Luca Agnetta, Michael Decker, José M. Lluch, Jordi Hernando, Pablo Loza-Alvarez, and Pau Gorostiza**

Abstract: To interrogate neural circuits and crack their codes, in vivo brain activity imaging must be combined with spatiotemporally precise stimulation in three dimensions using genetic or pharmacological specificity. This challenge requires deep penetration and focusing as provided by infrared light and multiphoton excitation, and has promoted two-photon photopharmacology and optogenetics. However, three-photon brain stimulation in vivo remains to be demonstrated. We report the regulation of neuronal activity in zebrafish larvae by three-photon excitation of a photoswitchable muscarinic agonist at 50 pM, a billion-fold lower concentration than used for uncaging, and with mid-infrared light of 1560 nm, the longest reported photoswitch wavelength. Robust, physiologically relevant photoresponses allow modulating brain activity in wild-type animals with spatiotemporal and pharmacological precision. Computational calculations predict that azobenzene-based ligands have high three-photon absorption cross-section and can be used directly with pulsed infrared light. The expansion of three-photon pharmacology will deeply impact basic neurobiology and neuromodulation phototherapies.

Introduction

To understand how (patho)physiological processes work, it is crucial to monitor activities of interest in vivo while manipulating specific molecular and cellular mechanisms and assessing their outcomes, including behavioral responses. For those purposes, in vivo and intravital microscopy technologies have proven useful virtually in every tissue and application from cancer[1] to infections,[2] including drug delivery.[3] These technologies have become particu-

[*] R. Sortino, F. Riefolo, C. Matera, P. Gorostiza
Institute for Bioengineering of Catalonia (IBEC), The Barcelona Institute for Science and Technology
08028 Barcelona (Spain)
E-mail: pau@icrea.cat

R. Sortino, F. Riefolo, C. Matera, N. Fernàndez-Castillo, P. Gorostiza
CIBER-BBN, ISCIII
28029 Madrid (Spain)

M. Cunquero, G. Castro-Olvera, P. Loza-Alvarez
ICFO—Institut de Ciencies Fotoniques, The Barcelona Institute of Science and Technology
08860 Castelldefels (Barcelona) (Spain)
E-mail: pablo.loza@icfo.eu

R. Gelabert, M. Moreno, J. M. Lluch, J. Hernando
Departament de Química, Universitat Autònoma de Barcelona (UAB)
08193 Bellaterra (Spain)

N. Fernàndez-Castillo
Departament de Genètica, Microbiologia i Estadística, Facultat de Biologia, Universitat de Barcelona
08028 Barcelona (Spain)

N. Fernàndez-Castillo
Institut de Biomedicina de la Universitat de Barcelona (IBUB)
08028 Barcelona (Spain)

N. Fernàndez-Castillo
Institut de Recerca Sant Joan de Déu (IRSJD)
08950 Esplugues de Llobregat (Spain)

L. Agnetta, M. Decker
Pharmaceutical and Medicinal Chemistry, Institute of Pharmacy and Food Chemistry, Ludwig Maximilian University of Würzburg
97074 Würzburg (Germany)

J. M. Lluch
Institut de Biotecnologia i de Biomedicina (IBB), UAB
08193 Bellaterra (Spain)

P. Gorostiza
Catalan Institution of Research and Advanced Studies (ICREA)
08010 Barcelona (Spain)

F. Riefolo
Current address: Teamit Institute, Partnerships, Barcelona Health Hub
08025 Barcelona (Spain)

C. Matera
Current address: Department of Pharmaceutical Sciences, University of Milan
20133 Milan (Italy)

larly appealing for interrogating and manipulating brain activity.[4]

Several approaches have been reported for activity imaging and stimulating deep in the brain[5] in vivo: (1) microendoscopy with gradient refractive index lenses that are invasively introduced in the tissue;[6] (2) adaptive optics, wavefront shaping methods[7] and refinements to reduce aberrations, phase- and motion-dependence; and (3) multiphoton excitation (MPE) using pulsed infrared (IR) light, which is weakly absorbed and scattered by the tissue, allowing fluorescence imaging of chemical and genetically encoded indicators, thus affording deep penetration and sharp focusing. The nonlinear process of simultaneous absorption of multiple photons by a molecule to reach an electronic state whose energy equals the sum of the photon energies[8] requires a high intensity of light. The advent of pulsed lasers[9] enabled fluorescence microscopy in the visible range using two-photon excitation (2PE) of IR light[10] and led to 2PE calcium and sodium imaging of neuronal activity.[11]

Depths of several hundred micrometers can be achieved by 2PE at wavelengths between 700–900 nm (near infrared NIR-I window).[12] However, this still only constitutes a fraction of the cortical thickness of mice (≈1 mm) and humans (up to ≈5 mm). Longer wavelengths in the 1300–1700 nm range (extending into the NIR-II window) allow even lower light absorption and scattering, making them potentially compatible with the same fluorescent reporters using three-photon excitation (3PE). As a rule of thumb, a chromophore with 400 nm excitation wavelength under continuous wave illumination (one-photon excitation, 1PE) can also be excited at 800 nm by 2PE and at 1200 nm by 3PE, provided the corresponding absorption cross-sections are sufficiently high.[13] Over the last decade, 3PE has drawn growing interest in neuroscience, facilitating whole cortex imaging[14] and neuronal activity imaging.[15]

To interrogate neural circuits and crack their codes, activity imaging must be combined with spatiotemporally precise stimulation in three dimensions, which requires the focusing provided by MPE. Two-photon (2P) optogenetics[16] and 2P photopharmacology, including caged[17] and photoswitchable ligands[18] have been recently developed and reviewed.[19] However, neuronal stimulation in vivo with 3PE has never been reported, either with optogenetics or with photopharmacology. This stands in contrast to the advances in 3PE compounds and materials for micromachining, bioimaging, and phototherapies.[20]

In this study, we aimed at manipulating a physiological process using 3PE, which we achieved by photopharmacological activation of neuroreceptors. Specifically, we report that M_2 muscarinic acetylcholine receptors (mAChRs) can be selectively activated in vitro and in vivo using a photoswitchable dualsteric ligand (phthalimide azobenzene iperoxo, PAI) at picomolar concentrations in the bath and 1560 nm pulsed light, which is the longest photoactivation wavelength reported to date. These results demonstrate the applicability of three-photon pharmacology (3PP) and set new uses for deep and focalized stimulation of cellular activity in vivo.

Results and Discussion

In previous work, we have demonstrated that *cis*-PAI can be pharmacologically activated and deactivated using continuous wave illumination under 1PE: excitation of its n→π* transition at 420–460 nm promotes the formation of the active *trans* isomer, while subsequent irradiation of its π→π* transition at 365 nm triggers photoisomerization towards the inactive *cis*-enriched configuration (Figure 1).[18d] In addition, we empirically applied 2PE to photoactivate PAI at approximately twice the wavelength of the 1PE n→π* transition (840 nm), which also induced its *cis*-to-*trans* isomerization and activated M_2 mAChR, thereby initiating intracellular calcium oscillations (Figure 1 and Supplementary Figure S1). We also noticed that such oscillations cannot be stopped with 730 nm pulsed light in the same range of peak power, suggesting that *trans*-to-*cis* isomerization by excitation of its π→π* transition is not an efficient process at 2PE (Supplementary Figure S1).

To understand and improve the penetration and focusing of azo-based photoswitchable drugs using MPE, we have herein examined the 1PE, 2PE, and 3PE properties of PAI using theoretical calculations. As far as we know, only a

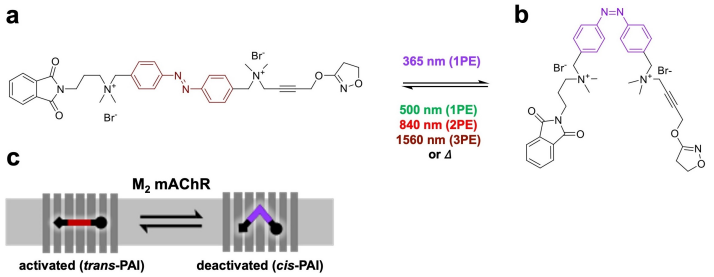

Figure 1. PAI (de)activates M_2 muscarinic acetylcholine receptors. 2D representation of the chemical structures of (a) *trans*-PAI and (b) *cis*-PAI. Photoisomerization between *trans* and *cis* can be achieved by 365 nm (1PE) and between *cis* and *trans* by 420–500 nm (1PE), 840 nm (2PE)[18d] and 1560 nm (3PE, this work). (c) Diagram depicting the 7 transmembrane receptor M_2 mAChR transitioning between the activated state in the presence of the ligand *trans*-PAI (left) and the deactivated state with *cis*-PAI (right). (Photo)activation of M_2 mAChR leads to cyclic (cAMP) decrease under physiological conditions. In this work, we have coupled M_2 mAChR activation to intracellular calcium release by means of the protein $G\alpha_{qTOP}$, to take advantage of calcium imaging in cell populations.[18d]

previous computational study has been reported on the high-order multiphoton absorption cross-sections (2P-5P) of centrosymmetric *trans*-azobenzenes (e.g., the azobenzene core of *trans*-PAI), which proposed different trends for the excitability of their odd- and even-order absorption processes. For *trans*-azo chromophores with an inversion center, the odd-photon absorption processes are largely determined by the one-photon absorption strength, whereas even-photon absorption processes are set by the 2P absorption strength.[21] Based on this precedent and the lack of previous similar studies on *cis*-azobenzenes, we focused our attention on PAI and two other simpler azobenzene models (Supplementary Figure S2), whose multiphoton absorption cross-sections were computed for both isomers using density functional theory calculations at the DFT/CAM-B3LYP level (Supporting Information Tables S1–S6 and Figures S3–S8). The reliability of this method was validated by our calculations of their 2PE properties, which predicted that their *cis*-to-*trans* photoisomerization should be more favoured than their *trans*-to-*cis* photoisomerization upon excitation with NIR-I radiation. Thus, larger 2P excitability was computed for the lower energy $n\rightarrow\pi^*$ ($\sigma_{2,cis}/\sigma_{2,trans}=11$) and $\pi\rightarrow\pi^*$ ($\sigma_{2,cis}/\sigma_{2,trans}=1660$) transitions of *cis*-PAI in relation to *trans*-PAI, which agrees with our experimental results (Supporting Information Tables S5 and S6). Indeed, we have shown an efficient photoconversion of *cis*-PAI to the pharmacologically active *trans* isomer using 2PE at 840 nm[18d] and the difficulty to deactivate *trans*-PAI using 2PE at 730 nm (Supplementary Figure S1). More interesting were our calculations of higher-order MPE of PAI like 3PE, which predict that its activation can be triggered using NIR-II wavelengths to achieve deeper distances into the tissues and even sharper focusing than 2PE.[14b] In particular, the results of the molecular computations indicate that the *cis*-to-*trans* photoisomerization of the centrosymmetric azobenzene is favored under 3PE of their $n\rightarrow\pi^*$ transition at around 1500 nm ($\sigma_{3,cis}/\sigma_{3,trans}=314$ for PAI; Supporting Information Tables S5 and S6). Overall, these data support the feasibility of 3PE to activate M_2 mAChRs.

To verify these predictions, we could not take advantage of the 2PE setup used in previous experiments,[18a,c–e] as the SpectraPhysics Mai Tai Ti:sapphire laser tuning range only reaches 920 nm. Thus, we built a custom multiphoton stimulation and fluorescence imaging setup (Supplementary Figure S16) based on an inverted microscope coupled to a femtosecond-pulsed laser beam (FFS, Toptica) that emits at a fixed wavelength of 1560 nm with a repetition rate of 100 MHz, a pulse duration of 120 fs, and allows a maximum peak power of 3.3 kW. Briefly, the optical system allows for imaging and tracking of the emitted fluorescence while photostimulating a region of interest.

In this setup, real-time calcium imaging assays were performed in transiently transfected HEK tsA201 cells coexpressing human M_2 mAChR and a chimeric $G\alpha_{q/i}$-protein ($G\alpha_{qTOP}$) in order to couple M_2 mAChR activation to the phospholipase C pathway, thus inducing inositol 1,4,5-trisphosphate (IP3) production and subsequent intracellular calcium release from the endoplasmic reticulum.[22] HEK cells were loaded with the fluorescent calcium indicator OGB-1 AM (see Methods section). We performed calcium imaging at 1PE and manipulated the activity of M_2 mAChRs with the reference agonist iperoxo (IPX)[23] and with PAI under 3PE conditions (1560 nm at the maximum available peak power). Application of *cis*-PAI (50 pM *trans*-PAI, pre-illuminated with 365 nm, Figure 1) did not elicit cellular responses, as reported.[18d] Remarkably, 3PE in the presence of *cis*-PAI induced a significant increase in intracellular calcium activity (Figure 2a), indicating that PAI was photoconverted to its *trans* form. The time course of calcium responses to 3PE of PAI displayed a diversity of behaviors in individual cells, such as oscillatory waves, transient peaks, and steps (Figure 2b). Similar intracellular responses have been previously observed in $G\alpha_q$-coupled GPCRs like metabotropic glutamate 5 receptors[24] and depend on the ratio of endogenous G protein and receptor overexpression level in each cell.[18c] M_2 mAChRs are naturally $G\alpha_i$-coupled, but these effects can be attributed to the overexpression of $G\alpha_{qTOP}$ used in our calcium imaging assay.

To reduce deviations due to this temporal dependence, responses under control conditions, under the application of *cis*-PAI, and upon photoswitching with 3PE (*trans*-PAI enriched form), were quantified both by peak amplitude and area under the curve (AUC). The analysis of these parameters showed that 3PE of PAI significantly stimulated the release of intracellular calcium, as much as IPX, and that its effect is absent without illumination (*cis*-PAI) (Figure 2cd). 3PE alone did not produce any stimulation artifacts ($n=9$, Supplementary Figure S9a). Photoresponses were also absent in cells not expressing M_2 mAChRs ($n=40$, Supplementary Figure S10). All these experiments confirm that the calcium responses observed upon 3PE are elicited by the specific interaction of the active isoform of PAI with M_2 mAChRs. Hence, *cis*-PAI can be photoswitched using 1560 nm light. In addition, as the amplitudes of the calcium signals elicited under 3PE were even higher than those previously reported by us upon 1PE of *cis*-PAI at 460 nm and similar experimental conditions ($\approx$50 % of IPX-induced responses), we conclude that irradiation at 1560 nm should indeed lead to efficient *cis*-to-*trans* photoswitching.[18d]

We further aimed to test the mechanism of PAI activation at this wavelength, and we studied the differences in cellular photoresponses concerning the photostimulation power, which is expected to follow a quadratic or cubic dependence for 2PE and 3PE, respectively. Using the same setup described above, the photoresponses were recorded at increasing laser power (63 %, 79 %, 91 %, and 100 %, the latter corresponding to an average power of 42 mW at the back focal plane of the cells). Average and example traces from individual cells are shown in Figure 3ab. 3PE alone did not produce any artifacts ($n=10$, Supplementary Figure S9b). We quantified the responses by AUC, maximum amplitude, and percentage of photoresponsive cells (Figure 3cd and Supplementary Figure S11ab). The power dependence of the AUC yields an exponential factor of 3.1 ($R^2=0.996$), unambiguously confirming that PAI photoisomerization at 1560 nm follows a third-order non-linear process (3PE). The amplitude and fraction of responding cells display similar values but lower correlation, probably

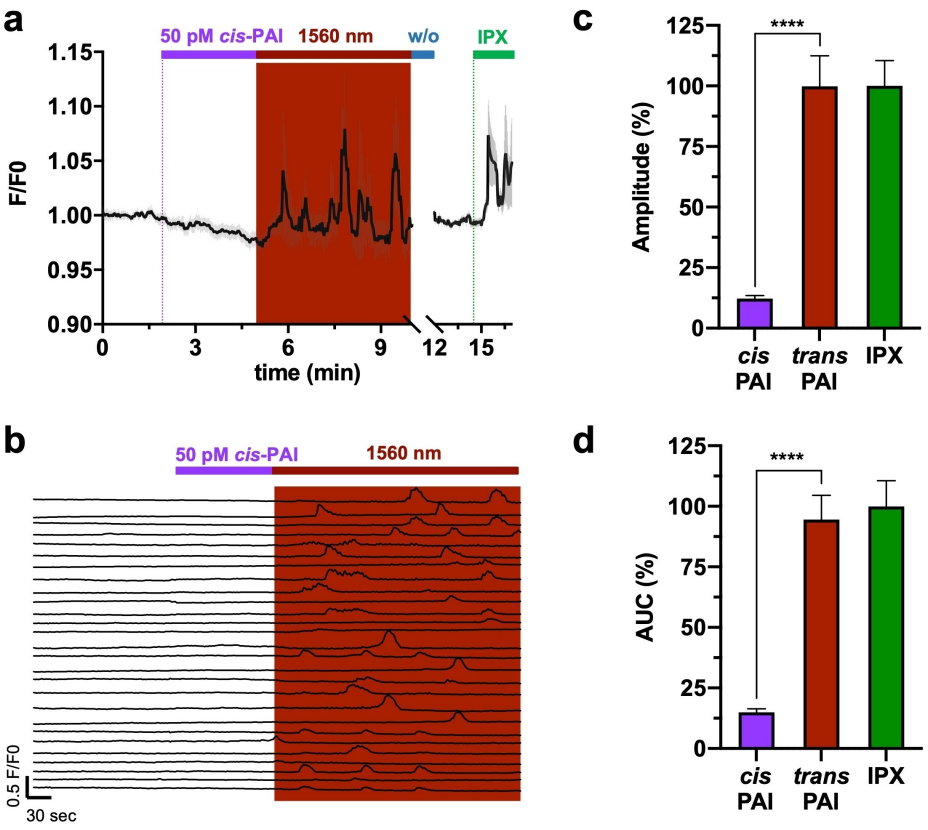

Figure 2. Activation of PAI with near-infrared (NIR) light under three-photon excitation (3PE). Real-time calcium imaging traces from HEK tsA201 cells coexpressing M_2 mAChR and $G\alpha_{qTOP}$, which were loaded with the calcium indicator OGB-1 AM (10 μM). (a) Average trace of cell responses to the subsequent application of (1) *cis*-PAI (50 pM) pre-illuminated at 365 nm (purple bar), (2) *trans*-enriched PAI obtained under 3PE at 1560 nm maximum power (dark red bar), and (3) the muscarinic agonist iperoxo (IPX, green bar) after manual wash-out (w/o, blue bar) ($n=9$ cells). Grey bands indicate the standard error of the mean (SEM). (b) Single cell calcium responses induced by PAI under 3PE at 1560 nm (dark red panel) (27 cells from 4 independent experiments). Purple bar indicates application of *cis*-PAI, dark red bar indicates illumination at 1560 nm. (c,d) The quantification is presented in the right graphs, where a significant response, in terms of (c) amplitude and (d) area under the curve (AUC) is observed upon the application of a pulsed NIR light (1560 nm) in the presence of PAI due to its photoisomerization to the *trans*-active form ($n=27$ cells from 4 independent experiments). Data were normalized to the average cell response to IPX and statistical significance was inferred by the one-way ANOVA with Tukey's multiple comparisons post-hoc test p-value (****) <0.0001; GraphPad Prism 9. Error bars are ± SEM.

due to the transient nature of the M_2-mediated cellular responses and the variable expression levels of M_2 mAChRs and $G\alpha_{qTOP}$ in individual cells.

We have previously shown that PAI can control cardiac function in tadpoles and rats,[18d] and brain wave activity in mice[25] through the use of continuous wave illumination (1PE). Recently, we demonstrated in vivo photoswitching by 2PE in invertebrates.[18e] To test 3PE in an animal model, we used zebrafish larvae expressing a genetically encoded calcium indicator, which made it possible to monitor brain activity (GCaMP6s) and to study the changes in calcium concentration upon photostimulation with the customized optical set-up described above (see Methods). Figure 4a shows an example of GCaMP6s fluorescence images, the zebrafish brain regions used for quantification, and the 3PE region in the field of view. Spontaneous neuronal activity was observed throughout the experiment and was not significantly affected by 3PE or by the application of 50 pM *cis*-PAI in the bath (see example frames in Figure 4b). However, 3PE in the presence of *cis*-PAI produced large calcium responses in all regions of the brain, including the activation of well-defined structures that will be the subject of a dedicated study (see the rightmost frame in Figure 4b). A representative movie is available as Supporting Information (Figure S15). The time course of calcium activity in different brain regions is shown in Figure 4c and the corresponding quantifications and dose-response curves (AUC and peak amplitude) are in Figures 4d, 4e and Supplementary Figure S12. Overall, a fourfold increase in neuronal activity was elicited by PAI using 3PE in vivo. This increase was significantly inhibited by the addition of AQ-RA 741[26] (an M_2 mAChRs selective antagonist), showing that *trans*-PAI acts on this specific receptor (Figure 4f).

These neuroexcitatory responses elicited by 3PE of PAI in vivo (Figure 4) are robust, physiologically relevant, and offer an unprecedented way to modulate brain activity in wildtype animals through M_2 mAChRs with high spatiotemporal resolution. In contrast, calcium responses in vitro (Figures 2 and 3) are weaker: 3PE responses are obtained from 25 % of the cells expressing M_2 mAChR (Figure S11a)

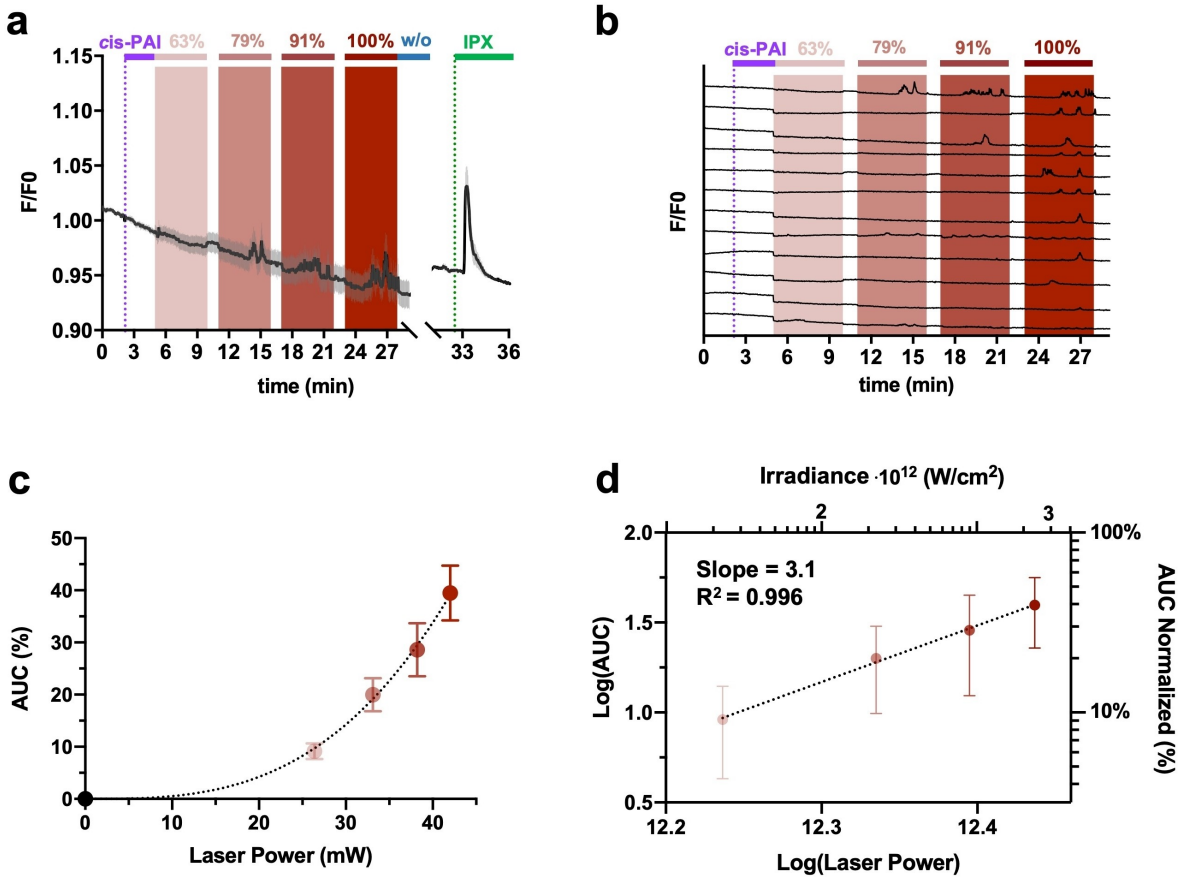

Figure 3. Dependence of the multiphoton photoresponse on average laser power. Real-time calcium imaging traces from HEK tsA201 cells coexpressing M_2 mAChR and $G\alpha_{qTOP}$, which were loaded with the calcium indicator OGB-1 AM (10 μM). (a) Average trace of cell responses to *cis*-PAI (50 pM, purple bar), *trans*-enriched PAI obtained under 3PE with different laser powers (63% light pink bar; 79% pink bar; 91% light red bar; 100% dark red bar, the latter corresponding to an average power of 42 mW at the back focal plane of the cells) and the muscarinic agonist iperoxo (IPX, green bar) after manual wash-out (w/o, blue bar) ($n=12$ cells). Grey band indicates SEM. (b) Single cell calcium responses induced by PAI (purple bar) under 3PE at 1560 nm with different laser power (63% light pink bar; 79% pink bar; 91% light red bar; 100% dark red bar, $n=12$ cells). (c) Photoresponse quantification as percent change of the area under the curve (AUC) as a function of average laser power at the back focal plane of the objective. Data have been normalized to the average cell response to IPX ($n=36$ cells from 4 independent experiments). The percentage of response versus power can be fitted by a cubic function, indicating that the process is mediated by 3PE. (d) Linear regression model using logarithmically transformed data of the irradiance (in $W\cdot cm^{-2}$). The R^2 of the fit is 0.996 and the slope is 3.1. Error bars are ± SEM.

and reach 40% of IPX responses at the maximum laser power (Figure S11b), probably due to the non-physiological coupling provided by $G\alpha_{qTOP}$. Nevertheless, these in vitro assays were convenient to set up and validate 3PE using high-throughput imaging rather than electrophysiological recordings in individual cells and may be useful to further refine the photoswitchable compounds and MPE optical system. Even the energy required to induce 3PE of PAI is orders of magnitude below the energy reported[27] in studies of optogenetic stimulation in cultured neurons (Supplementary Figure S14) (50 mW to fire an action potential, 64 mW to produce photodamage).[28]

The results obtained with 2PE (Figure 5 in reference [18d] and Supplementary Figure S1 in this work) agree with our calculations of the multiphotonic properties of PAI: the lower energy n→π* and π→π* transitions in *cis*-PAI are more favored than in *trans*-PAI under 2PE, elucidating why only *cis*-to-*trans* photoisomerization of PAI can be efficiently induced with 700–900 nm NIR-I radiation, whereas the reversible operation of the photoswitch within this spectral range is less encouraged. In contrast, our calculations for PAI and simpler azobenzenes predict a reversible behavior under 3PE. Their 3PE absorption cross-sections for the n→π* transition at around 1500 nm are much larger for the *cis* isomer compared to the *trans* one, ensuring effective *cis*-to-*trans* photoisomerization, as conclusively demonstrated for PAI by our photopharmacology data in Figures 2–4. Here, this situation appears reversible for the π→π* transition with 3PE, which we computed to be more probable for the *trans* isomer of these azo compounds compared to the corresponding 2PE transition ($\sigma^{\pi\to\pi^*}_{3,trans}/\sigma^{\pi\to\pi^*}_{3,cis}=83$) for PAI; Supporting Information Tables S5 and S6). This combined computational and experimental study raises hopes of strong and reversible responses for 3PE of all electronically-symmetric *trans*-azo-based photoswitchable drugs. In addition, it should enable rever-

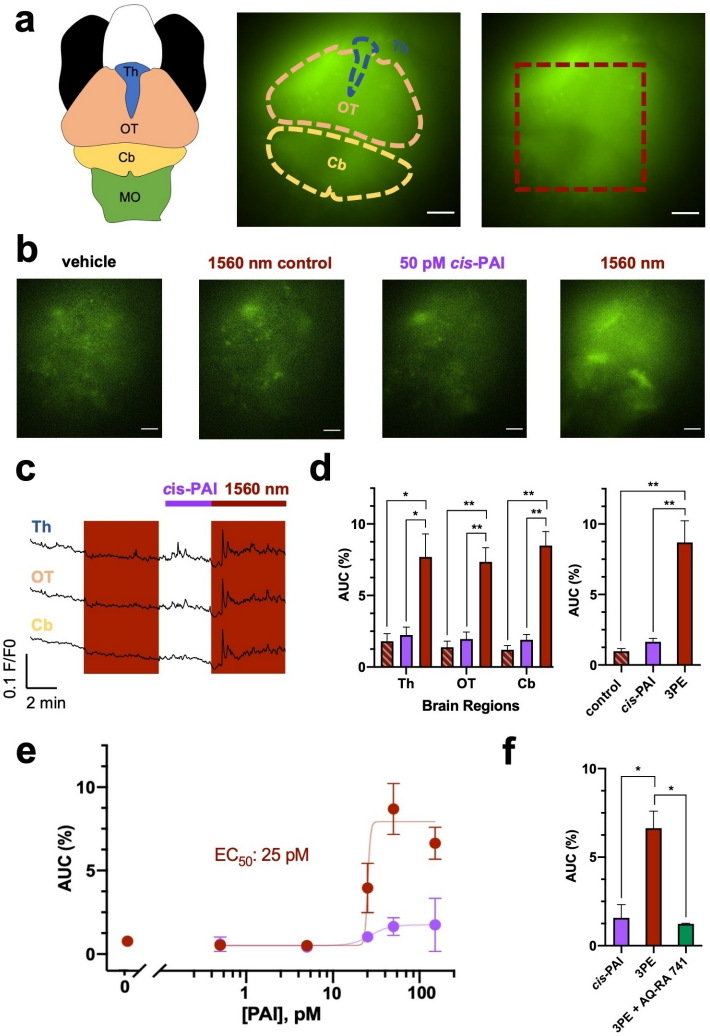

Figure 4. In vivo activation of PAI by three-photon excitation (3PE). Green fluorescence signal from GCaMP6s indicator upon different conditions. (a) Sketch of the main regions of the zebrafish larva brain (dorsal view): Th, thalamus; OT, optic tectum; Cb, cerebellum; MO, medulla oblongata. Among these regions, three were visible as shown in the middle figure from zebrafish larvae expressing the calcium indicator GCaMP6s. The region illuminated with the 3PE laser (red dashed line) is represented on the right. The scale bar represents 50 μm. (b) Representative images of different experimental conditions. No effects were observed with the vehicle and with pulsed-laser irradiation (1560 nm) prior to adding the drugs. The application of 50 pM *cis*-PAI alone did not change neuronal activity, but upon pulsed-laser irradiation, large photoresponses were observed presumably due to isomerization to the *trans*-PAI form. The scale bar represents 50 μm. (c) Real-time fluorescence calcium imaging traces from different brain regions (Th, OT and Cb) under the conditions described in (b). The transient and oscillatory response elicited by 3PE of PAI is observed in all regions. (d) Quantification of photoresponses in separate regions and averaged response over the whole brain ($n=5$ independent experiments). Striped bars indicate 3PE in the absence of drug, purple bars indicate the application of 50 pM *cis*-PAI, and dark red bars indicate photoresponses to 3PE (photoswitching to *trans*-PAI using 1560 nm light). (e) Dose-response curves of *trans*-PAI obtained under 3PE (red line) and *cis*-PAI pre-irradiated with UV light (violet line). The concentration-dependent responses are plotted as area under the curve (%). Amplitude responses are shown in Supplementary Figure S12c. The concentrations used were: 0.5 ($n=3$), 5 ($n=3$), 25 ($n=3$), 50 ($n=5$) and 150 ($n=3$) pM of PAI. The 3PE light control is represented as a red dot. The EC_{50} values determined for *trans*-PAI and *cis*-PAI are 25 pM and 43 pM, respectively. Error bars indicate SEM. The curves were obtained by nonlinear regression analysis with variable slope using GraphPad Prism. (f) Calcium responses induced by the 3PE of PAI (150 pM) are abolished by the addition of AQ-RA 741, a M_2 mAChR selective antagonist (1 μM) ($n=3$). Data in panels d and f were analyzed by the paired t-test (p-value (**) <0.01 and p-value (*) <0.05 using GraphPad Prism 9). Error bars indicate $\pm$SEM.

sible full-3PE operation of these compounds by orthogonally exciting their $\pi\rightarrow\pi^*$ and $n\rightarrow\pi^*$ transitions with NIR-II radiation to selectively trigger *trans*-to-*cis* and *cis*-to-*trans* photoconversion, respectively. Unfortunately, we have not yet tested this prediction experimentally due to the limited wavelength range of our pulsed lasers (700–900 nm tunable MaiTai and 1560 nm fixed wavelength Toptica).

Note that centrosymmetric azobenzenes make up a large portion of photochromic groups used in photopharmacology[29] and often display slow thermal relaxation and higher potency in *trans* configuration. Therefore, our results suggest that they could be used directly for 3PE with NIR-II light to take advantage of enhanced tissue penetration and focusing.[14–15,30] To further validate this

approach, we decided to perform the in vivo experiments with another photoswitchable molecule bearing an azoaromatic chromophore that targets a different receptor. Based on theoretical calculations, for this purpose we selected benzyl quinolone carboxylic acid-azo-iperoxo (BQCAAI[31] or BAI for simplicity), which is a photoswitchable agonist of M_1 receptors that activates them in its *trans* form under 1PE (460 nm). According to DFT/CAM-B3LYP computations, BAI should also present favored *cis*-to-*trans* photoisomerization by 3PE around 1500 nm (Supplementary Figure S2 and Tables S7 and S8). We carried out in vivo experiments applying *cis*-BAI (pre-irradiated with UV light) at micromolar concentrations in the bath and observed that 3PE increased calcium fluorescence responses in the zebrafish brain. The corresponding dose-response plots (AUC and peak amplitude) are presented in Supplementary Figure S13.

In addition, this behavior could be expanded to photopharmacological compounds based on electronically-asymmetric azobenzenes,[18a–b,e] as asymmetric chromophores featuring electron donors and acceptors also display high absorption cross-sections at 3PE.[32] Therefore, the wide application of 3PP would have a deep impact in the field as well as in chemical biology and phototherapies. These results may be relevant for multiphoton lithography[33] and polymerization[34] as well. A few 3PE studies have been reported for optogenetics[27] and caged compounds.[35] These potentially alternative 3PE methods would have advantages of their own (e.g., genetic targeting and release of physiological ligands, respectively); however, they display relatively low 3PE efficacy. The three-photon (3P) uncaging cross-section reported for these systems at 1064 nm ($\sigma_{3,uncaging} = 4.0 \cdot 10^{-85}$ cm^{6}s^2 photon^{-2})[35] is several orders of magnitude lower than the 3P absorption cross-section computed for PAI at around 1500 nm ($\sigma_{3,cis} = 1.8 \cdot 10^{-77}$ cm^{6}s^{2}photon^{-2}), while the irradiance required for 3P optogenetic manipulation[27] is considerably larger than for 3P PAI photocontrol (Supplementary Figure S14). As a result, high overexpression levels or compound concentration may be required, leading to physiological disturbance (e.g., altering the microstructure and composition of dendritic spines)[36] and unintended pharmacological effects (e.g., $GABA_AR$ blockade in the case of caged glutamate prior to release).[37] As a reference, 2PE absorption cross-sections have been discussed for photopharmacology, including reversible photoswitches and caged compounds.

The multiphoton absorption cross-section of a photoswitchable ligand can be complemented by a Figure of merit of its practical usability in 3PE: 50 pM *cis*-PAI (above its EC_{50})[18d] allows, by 3PE photoactivation, nearly half of the maximal IPX responses at a power density that does not produce unspecific effects in neurons. This suggests that improving pharmacological potency (potentially reaching the femtomolar range) may be as beneficial as increasing the multiphoton cross-section to achieve highly sensitive photopharmacological compounds. Thus, when targeting endogenous receptors in vivo with 3PE, azobenzene photoswitches provide excellent performance. If optogenetic manipulation with 3PE[27] is of interest, genetically targeted azobenzene photoswitches like LiGluR[38] offer a convenient option. The concentration used in our 3PE assays with PAI (50 pM) is $\approx 10^9$ times lower than that required for 2PE glutamate uncaging in vivo (20 mM).[39]

The wavelength used in our experiments (1560 nm) allows effectively photoisomerizing PAI to the active form using 3PE. However, light is also strongly absorbed by water in this spectral range,[40] suggesting that wavelengths lying at lower absorption bands like 1300 nm or 1700 nm generally used for 3PE imaging may yield even better results, provided that the photoswitch absorption band for third-order processes is sufficiently wide.

Conclusion

In summary, we report the first method to control brain activity in vivo using 3PE and mid-IR light. It is based on the photopharmacological activation of mAChRs by means of the photoswitchable ligand PAI at 50 pM and 1560 nm light, which are respectively the lowest concentration and the longest photoactivation wavelength ever reported. In addition, we provide experimental assays to characterize their performance and theoretical guidelines for further optimization. Our calculations predict that most photoswitchable ligands used in 1PE photopharmacology with UV and visible light (symmetric and asymmetric azobenzenes) are suitable for 3PE with mid-IR light and can benefit from enhanced tissue penetration and focusing. The wide application of 3PP would be transformative for basic research in neurobiology and to progress advanced neuromodulation therapies based on light.

Acknowledgements

We are grateful to Chris Xu, Julien Colombelli, and Elena Rebollo for useful discussions, to Jean-Philippe Pin for the $G\alpha_{qTOP}$ clone, and to Sarah Moreira for revising the manuscript. GCaMP6s albino zebrafish embryos were generated by the National Institute of Genetics (Japan) and obtained from Matt Parker. This research received funding from the European Union Research and Innovation Programme Horizon 2020—Human Brain Project SG3 (945539), DEEPER (ICT-36-2020-101016787), Agency for Management of University and Research Grants/Generalitat de Catalunya (CERCA Programme; 2021-SGR-01410; 2021-SGR-00064), Fonds Européen de Développement Économique et Régional (FEDER) funds, Ministry of Science and Innovation grants PID2019-111493RB-I00 (DEEP RED), PID2022-142609OB-I00 (EPILLUM), and PID2020-113764GB-I00, Fundaluce and "la Caixa" foundations (ID 100010434, agreement LCF/PR/HR19/52160010). R. S. was supported by a predoctoral fellowship FPI (reference BES-2017-082496). M.C. acknowledges funding from Fondo Social Europeo (PRE2020-095721), M.C., G.C.O and P.L.A acknowledge funding form the Spanish Ministry of Economy and Competitiveness through the "Severo Ochoa" program for Centres of Excellence in R&D (CEX2019-000910-S),

from Fundació Privada Cellex, Fundació Mir-Puig, Generalitat de Catalunya through the CERCA program European Union's Horizon 2020 research and innovation programme under grant agreement No 871277 and Laserlab-Europe EU-H2020 (871124).

Conflict of Interest

The authors declare no conflict of interest.

Data Availability Statement

The data that support the findings of this study are available in the supplementary material of this article.

Keywords: Azobenzene · Multiphoton Excitation · Muscarinic Neuromodulation · Photopharmacology · Two-Photon Lithography and Polymerization

[1] a) R. K. Jain, L. L. Munn, D. Fukumura, *Nat. Rev. Cancer* **2002**, *2*, 266–276; b) L. Perrin, B. Bayarmagnai, B. Gligorijevic, *Cancer Rep.* **2020**, *3*, e1192.

[2] a) B. Stolp, K. Melican, *FEBS Lett.* **2016**, *590*, 2014–2026; b) X. Sewald, *Viruses* **2018**, *10*, 337.

[3] P. Amornphimoltham, A. Masedunskas, R. Weigert, *Adv. Drug Delivery Rev.* **2011**, *63*, 119–128.

[4] a) J. Grutzendler, N. Kasthuri, W. B. Gan, *Nature* **2002**, *420*, 812–816; b) A. K. Majewska, J. R. Newton, M. Sur, *J. Neurosci.* **2006**, *26*, 3021–3029; c) E. J. Yoder, D. Kleinfeld, *Microsc. Res. Tech.* **2002**, *56*, 304–305; d) C. Stosiek, O. Garaschuk, K. Holthoff, A. Konnerth, *Proc. Natl. Acad. Sci. USA* **2003**, *100*, 7319–7324.

[5] A. S. Abdelfattah, S. Ahuja, T. Akkin, S. R. Allu, J. Brake, D. A. Boas, E. M. Buckley, R. E. Campbell, A. I. Chen, X. Cheng, T. Cizmar, I. Costantini, M. De Vittorio, A. Devor, P. R. Doran, M. El Khatib, V. Emiliani, N. Fomin-Thunemann, Y. Fainman, T. Fernandez-Alfonso, C. G. L. Ferri, A. Gilad, X. Han, A. Harris, E. M. C. Hillman, U. Hochgeschwender, M. G. Holt, N. Ji, K. Kilic, E. M. R. Lake, L. Li, T. Li, P. Machler, E. W. Miller, R. C. Mesquita, K. Nadella, U. V. Nagerl, Y. Nasu, A. Nimmerjahn, P. Ondrackova, F. S. Pavone, C. Perez Campos, D. S. Peterka, F. Pisano, F. Pisanello, F. Puppo, B. L. Sabatini, S. Sadegh, S. Sakadzic, S. Shoham, S. N. Shroff, R. A. Silver, R. R. Sims, S. L. Smith, V. J. Srinivasan, M. Thunemann, L. Tian, L. Tian, T. Troxler, A. Valera, A. Vaziri, S. A. Vinogradov, F. Vitale, L. V. Wang, H. Uhlirova, C. Xu, C. Yang, M. H. Yang, G. Yellen, O. Yizhar, Y. Zhao, *Neurophotonics* **2022**, *9*, 013001.

[6] a) J. C. Jung, A. D. Mehta, E. Aksay, R. Stepnoski, M. J. Schnitzer, *J. Neurophysiol.* **2004**, *92*, 3121–3133; b) M. Murayama, M. E. Larkum, *Nat. Protoc.* **2009**, *4*, 1551–1559; c) M. E. Bocarsly, W. C. Jiang, C. Wang, J. T. Dudman, N. Ji, Y. Aponte, *Biomed. Opt. Express* **2015**, *6*, 4546–4556.

[7] a) N. Ji, T. R. Sato, E. Betzig, *Proc. Natl. Acad. Sci. USA* **2012**, *109*, 22–27; b) N. Ji, *Nat. Methods* **2017**, *14*, 374–380; c) E. Papagiakoumou, F. Anselmi, A. Begue, V. de Sars, J. Gluckstad, E. Y. Isacoff, V. Emiliani, *Nat. Methods* **2010**, *7*, 848–854; d) E. Papagiakoumou, E. Ronzitti, V. Emiliani, *Nat. Methods* **2020**, *17*, 571–581; e) R. Aviles-Espinosa, J. Andilla, R. Porcar-Guezenec, O. E. Olarte, M. Nieto, X. Levecq, D. Artigas, P. Loza-Alvarez, *Biomed. Opt. Express* **2011**, *2*, 3135–3149.

[8] M. Göppert-Mayer, *Ann. Phys.* **1931**, *401*, 273–294.

[9] a) D. Strickland, G. Mourou, *Opt. Commun.* **1985**, *56*, 219–221; b) D. E. Spence, P. N. Kean, W. Sibbett, *Opt. Lett.* **1991**, *16*, 42–44.

[10] W. Denk, J. H. Strickler, W. W. Webb, *Science* **1990**, *248*, 73–76.

[11] W. Denk, K. R. Delaney, A. Gelperin, D. Kleinfeld, B. W. Strowbridge, D. W. Tank, R. Yuste, *J. Neurosci. Methods* **1994**, *54*, 151–162.

[12] A. N. Yaroslavsky, P. C. Schulze, I. V. Yaroslavsky, R. Schober, F. Ulrich, H. J. Schwarzmaier, *Phys. Med. Biol.* **2002**, *47*, 2059–2073.

[13] C. Xu, W. W. Webb, *Multiphoton Excitation of Molecular Fluorophores and Nonlinear Laser Microscopy, Vol. 5*, Springer, Berlin **2002**.

[14] a) N. G. Horton, K. Wang, D. Kobat, C. G. Clark, F. W. Wise, C. B. Schaffer, C. Xu, *Nat. Photonics* **2013**, *7*, 205–209; b) K. Guesmi, L. Abdeladim, S. Tozer, P. Mahou, T. Kumamoto, K. Jurkus, P. Rigaud, K. Loulier, N. Dray, P. Georges, M. Hanna, J. Livet, W. Supatto, E. Beaurepaire, F. Druon, *Light-Sci. Appl.* **2018**, *7*, 12.

[15] a) D. G. Ouzounov, T. Wang, M. Wang, D. D. Feng, N. G. Horton, J. C. Cruz-Hernandez, Y. T. Cheng, J. Reimer, A. S. Tolias, N. Nishimura, C. Xu, *Nat. Methods* **2017**, *14*, 388–390; b) A. Klioutchnikov, D. J. Wallace, J. Sawinski, K. M. Voit, Y. Groemping, J. N. D. Kerr, *Nat. Methods* **2022**, *20*, 610–616.

[16] a) J. P. Rickgauer, D. W. Tank, *Proc. Natl. Acad. Sci. USA* **2009**, *106*, 15025–15030; b) A. Begue, E. Papagiakoumou, B. Leshem, R. Conti, L. Enke, D. Oron, V. Emiliani, *Biomed. Opt. Express* **2013**, *4*, 2869–2879; c) M. Klausen, M. Blanchard-Desce, *J. Photochem. Photobiol. C* **2021**, *48*, 100423.

[17] a) W. Denk, *Proc. Natl. Acad. Sci. USA* **1994**, *91*, 6629–6633; b) G. C. R. Ellis-Davies, *Front. Synaptic Neurosci.* **2019**, *10*, 48.

[18] a) M. Izquierdo-Serra, M. Gascon-Moya, J. J. Hirtz, S. Pittolo, K. E. Poskanzer, E. Ferrer, R. Alibes, F. Busque, R. Yuste, J. Hernando, P. Gorostiza, *J. Am. Chem. Soc.* **2014**, *136*, 8693–8701; b) E. C. Carroll, S. Berlin, J. Levitz, M. A. Kienzler, Z. Yuan, D. Madsen, D. S. Larsen, E. Y. Isacoff, *Proc. Natl. Acad. Sci. USA* **2015**, *112*, E776–785; c) S. Pittolo, H. Lee, A. Llado, S. Tosi, M. Bosch, L. Bardia, X. Gomez-Santacana, A. Llebaria, E. Soriano, J. Colombelli, K. E. Poskanzer, G. Perea, P. Gorostiza, *Proc. Natl. Acad. Sci. USA* **2019**, *116*, 13680–13689; d) F. Riefolo, C. Matera, A. Garrido-Charles, A. M. J. Gomila, R. Sortino, L. Agnetta, E. Claro, R. Masgrau, U. Holzgrabe, M. Batlle, M. Decker, E. Guasch, P. Gorostiza, *J. Am. Chem. Soc.* **2019**, *141*, 7628–7636; e) G. Cabre, A. Garrido-Charles, M. Moreno, M. Bosch, M. Porta-de-la-Riva, M. Krieg, M. Gascon-Moya, N. Camarero, R. Gelabert, J. M. Lluch, F. Busque, J. Hernando, P. Gorostiza, R. Alibes, *Nat. Commun.* **2019**, *10*, 907.

[19] a) I. W. Chen, E. Papagiakoumou, V. Emiliani, *Curr. Opin. Neurobiol.* **2018**, *50*, 179–189; b) H. Adesnik, L. Abdeladim, *Nat. Neurosci.* **2021**, *24*, 1356–1366; c) M. Dudek, N. Tarnowicz-Staniak, M. Deiana, Z. Pokladek, M. Samoc, K. Matczyszyn, *RSC Adv.* **2020**, *10*, 40489–40507; d) S. Kellner, S. Berlin, *Appl. Sci.* **2020**, *10*, 805; e) F. A. Jerca, V. V. Jerca, R. Hoogenboom, *Nat. Chem. Rev.* **2022**, *6*, 51–69.

[20] a) L. Zhang, M. Morshedi, M. S. Kodikara, M. G. Humphrey, *Angew. Chem. Int. Ed.* **2022**, *61*, e202208168; b) B. Li, X. Lu, Y. Tian, D. Li, *Angew. Chem. Int. Ed.* **2022**, *61*, e202206755; c) C. Jin, F. Liang, J. Wang, L. Wang, J. Liu, X. Liao, T. W. Rees, B. Yuan, H. Wang, Y. Shen, Z. Pei, L. Ji, H. Chao, *Angew. Chem. Int. Ed.* **2020**, *59*, 15987–15991; d) Z. Xu, Z. Zhang, X. Deng, J. Li, Y. Jiang, W.-C. Law, C. Yang, W. Zhang, X. Chen, K. Wang, D. Wang, G. Xu, *ACS Nano* **2022**, *16*, 6712–6724.

[21] D. H. Friese, R. Bast, K. Ruud, *ACS Photonics* **2015**, *2*, 572–577.
[22] J. Gomeza, S. Mary, I. Brabet, M. L. Parmentier, S. Restituito, J. Bockaert, J. P. Pin, *Mol. Pharmacol.* **1996**, *50*, 923–930.
[23] R. Schrage, W. K. Seemann, J. Klockner, C. Dallanoce, K. Racke, E. Kostenis, M. De Amici, U. Holzgrabe, K. Mohr, *Br. J. Pharmacol.* **2013**, *169*, 357–370.
[24] S. Pittolo, X. Gomez-Santacana, K. Eckelt, X. Rovira, J. Dalton, C. Goudet, J. P. Pin, A. Llobet, J. Giraldo, A. Llebaria, P. Gorostiza, *Nat. Chem. Biol.* **2014**, *10*, 813–815.
[25] A. Barbero-Castillo, F. Riefolo, C. Matera, S. Caldas-Martinez, P. Mateos-Aparicio, J. F. Weinert, A. Garrido-Charles, E. Claro, M. V. Sanchez-Vives, P. Gorostiza, *Adv. Sci.* **2021**, *8*, e2005027.
[26] a) H. Doods, M. Entzeroth, N. Mayer, *Eur. J. Pharmacol.* **1991**, *192*, 147–152; b) H. N. Doods, M. Entzeroth, H. Ziegler, N. Mayer, P. Holzer, *Eur. J. Pharmacol.* **1994**, *253*, 275–281; c) F. Dörje, J. Wess, G. Lambrecht, R. Tacke, E. Mutschler, M. R. Brann, *J. Pharmacol. Exp. Ther.* **1991**, *256*, 727–733.
[27] C. J. Rowlands, D. Park, O. T. Bruns, K. D. Piatkevich, D. Fukumura, R. K. Jain, M. G. Bawendi, E. S. Boyden, P. T. So, *Light-Sci. Appl.* **2017**, *6*, e16255.
[28] P. Loza-Alvarez, D. Artigas, R. Aviles-Espinosa, *Semiconductor Lasers and Diode-based Light Sources for Biophotonics*, The Institution of Engineering and Technology **2018**.
[29] M. Wijtmans, I. Josimovic, H. F. Vischer, R. Leurs, *Curr. Opin. Pharmacol.* **2022**, *63*, 102192.
[30] A. Klioutchnikov, D. J. Wallace, M. H. Frosz, R. Zeltner, J. Sawinski, V. Pawlak, K. M. Voit, P. S. J. Russell, J. N. D. Kerr, *Nat. Methods* **2020**, *17*, 509–513.
[31] a) L. Agnetta, M. Kauk, M. C. A. Canizal, R. Messerer, U. Holzgrabe, C. Hoffmann, M. Decker, *Angew. Chem. Int. Ed.* **2017**, *56*, 7282–7287; b) J. M. Sanchez-Sanchez, F. Riefolo, A. Barbero-Castillo, R. Sortino, L. Agnetta, A. Manasanch, C. Matera, M. Bosch, M. Forcella, M. Decker, P. Gorostiza, M. Sanchez-Vives, **Submitted**.
[32] a) A. K. Mandal, S. Sreejith, T. He, S. K. Maji, X. J. Wang, S. L. Ong, J. Joseph, H. Sun, Y. Zhao, *ACS Nano* **2015**, *9*, 4796–4805; b) P. Cronstrand, B. Jansik, D. Jonsson, Y. Luo, H. Agren, *J. Chem. Phys.* **2004**, *121*, 9239–9246.
[33] a) S. Juodkazis, V. Mizeikis, K. K. Seet, M. Miwa, H. Misawa, *Nanotechnology* **2005**, *16*; b) Y. Markushyna, A. Savateev, *Eur. J. Org. Chem.* **2022**, *2022*, e202200026.
[34] B. H. Cumpston, S. P. Ananthavel, S. Barlow, S. M. Marder, P. J. W, *Nature* **1999**, *398*, 51–54.
[35] I. Tekeli, I. Aujard, X. Trepat, L. Jullien, A. Raya, D. Zalvidea, *Light-Sci. Appl.* **2016**, *5*, e16084.
[36] B. D. Allen, A. C. Singer, E. S. Boyden, *Learn. Mem.* **2015**, *22*, 232–238.
[37] W. Maier, J. E. Corrie, G. Papageorgiou, B. Laube, C. Grewer, *J. Neurosci. Methods* **2005**, *142*, 1–9.
[38] a) M. Volgraf, P. Gorostiza, R. Numano, R. H. Kramer, E. Y. Isacoff, D. Trauner, *Nat. Chem. Biol.* **2006**, *2*, 47–52; b) P. Gorostiza, M. Volgraf, R. Numano, S. Szobota, D. Trauner, E. Y. Isacoff, *Proc. Natl. Acad. Sci. USA* **2007**, *104*, 10865–10870; c) S. Szobota, P. Gorostiza, F. Del Bene, C. Wyart, D. L. Fortin, K. D. Kolstad, O. Tulyathan, M. Volgraf, R. Numano, H. L. Aaron, E. K. Scott, R. H. Kramer, J. Flannery, H. Baier, D. Trauner, E. Y. Isacoff, *Neuron* **2007**, *54*, 535–545; d) R. Numano, S. Szobota, A. Y. Lau, P. Gorostiza, M. Volgraf, B. Roux, D. Trauner, E. Y. Isacoff, *Proc. Natl. Acad. Sci. USA* **2009**, *106*, 6814–6819.
[39] J. Noguchi, A. Nagaoka, T. Hayama, H. Ucar, S. Yagishita, N. Takahashi, H. Kasai, *Sci. Rep.* **2019**, *9*, 13922.
[40] M. Wang, C. Wu, D. Sinefeld, B. Li, F. Xia, C. Xu, *Biomed. Opt. Express* **2018**, *9*, 3534–3543.

Manuscript received: August 2, 2023
Accepted manuscript online: October 12, 2023
Version of record online: November 20, 2023